Growth, structure, and magnetism of fcc Fe ultrathin films on Cu(111) by pulsed laser deposition

P. Ohresser, J. Shen,* J. Barthel, M. Zheng, Ch. V. Mohan, M. Klaua, and J. Kirschner
Max-Planck Institut für Mikrostrukturphysik, Weinberg 2, D-06120 Halle/Saale, Germany
(Received 24 August 1998)

Ultrathin Fe films on Cu(111) have been grown by pulsed-laser deposition (PLD) whose instantaneous deposition rate is about six orders of magnitude larger than that of the conventional molecular-beam epitaxy based on thermal deposition (TD). Compared to the TD prepared Fe/Cu(111) films, the PLD films have a significantly improved layer-by-layer morphology and a substantially enhanced stability of the fcc phase as characterized by scanning tunneling microscopy and electron-diffraction techniques. The magnetic properties of the PLD films, investigated by magneto-optical Kerr effect, also show remarkably different behavior as compared to the TD films. At low thickness (<3 ML), while the TD films are characterized by a low net moment and a short-range ferromagnetic order, the PLD films show a high net moment with a true long-range ferromagnetic order. Above 3 ML both PLD and TD films undergo a magnetic transition though with apparently different structural origin. We discuss these results based on the different growth and structure between the PLD and TD grown Fe films. [S0163-1829(99)02802-7]

I. INTRODUCTION

The magnetism of face-centered-cubic (fcc) γ-Fe has attracted great interest for decades. While theories pointed out that the ground state of fcc Fe is that of a spin-spiral density wave,[1] it is also well known that the spin structure of fcc Fe depends strongly on its lattice constant. Generally for the γ-Fe a larger lattice constant favors a larger magnetic moment as well as ferromagnetic exchange coupling. From the application point of view, it is most desirable to achieve ferromagnetic fcc Fe with high magnetic moment. This, however, appears to be impossible for bulk due to the difficulty of stabilizing γ-Fe at low temperatures, because its natural fcc phase exists only at temperatures (>1186 K) above the Curie temperature. A possible way to stabilize bulk γ-Fe at room temperature or below is forming precipitates in an fcc Cu matrix,[2] though they were observed to be antiferromagnetic with a Néel temperature of 67 K.[3]

Another approach to obtain high-moment ferromagnetic fcc Fe is to epitaxially grow Fe films on fcc substrates such as Ni, Cu, and Cu_3Au, whose lattice constants are close to that of Fe. Among them, Cu is the most interesting substrate because according to one calculation,[4] its lattice constant (3.61 Å) is just in between that of an antiferromagnetic phase and the high-moment ferromagnetic phase of fcc Fe. This has given hope to the achievement of ferromagnetic fcc Fe/Cu films. Experimental results indicate that the situation is rather complex. On the Cu(100) a ferromagnetic phase with a large net magnetic moment ($\sim 2.5\mu_B$) was indeed observed up to 4 monolayers (ML).[5] But in this thickness range the γ-Fe phase is in fact tetragonally expanded leading to an fct rather than an fcc structure.[6] Above 4 ML an fct to an fcc structural transformation takes place with the net moment falling down and staying around a constant value up to the bcc transformation thickness (~ 11 ML).[7] For this system the high moment is therefore linked to the fct phase instead of the fcc phase. In contrast the Cu(111) allows the growth of a nearly isotropic fcc Fe below approximately 3–4 ML.[8] But different experiments on copper capped films[9] and films grown on stepped surface[10] using thermal deposition indicate a small moment for the Fe of the order of $0.5\mu_B$. It is thus of great interest to study whether high-moment ferromagnetic Fe/Cu films with a true fcc structure can be achieved.

Recently we have found that high-moment ferromagnetic Fe films with fcc structure (below 4 ML) can be obtained when the films are grown on Cu(100) by pulsed-laser deposition (PLD).[11] Compared to the conventional molecular-beam epitaxy (MBE) method which is based on the thermal deposition (TD), the PLD technique has a remarkably high instantaneous deposition rate, i.e., the time scale of one laser pulse (typically several tens of nanoseconds) the rate is more than five orders of magnitude larger than the TD rate. The high deposition rate results in a high nucleation density, which in turn leads to a significantly improved two-dimensional growth of the PLD films. Although it is still under investigation whether the fcc structure of the PLD Fe/Cu(100) films is a direct consequence of the improved morphology, it is clear that the fcc PLD Fe/Cu(100) films have a similar high-moment ferromagnetic phase as the fct TD Fe/Cu(100) films.

In the present work we apply the PLD technique to grow Fe films on the Cu(111) substrate. The fact that the ultrafast PLD improves the growth of the films towards layer-by-layer is particularly useful for the Fe/Cu(111) system, since the thermal deposition leads to a three-dimensional island morphology with a clear tendency towards step decoration, provided the growth temperature is kept between 100 and 300 K. Depositing films at substrate temperatures below 100 K might improve the smoothness of the film, but the films grow directly in a bcc phase rather than an fcc phase.[12] For films grown at higher substrate temperature, a significant interdiffusion between Fe and Cu is unavoidable hindering the study of a well-defined system.[13] In our previous work we have reported that with the help of PLD, at early stages of growth the Fe films show a clear two-dimensional morphology with-

out any step decoration effect.[14] Here we extend our study to PLD grown Fe/Cu(111) films at higher thickness. We will demonstrate that the layer-by-layer growth of the PLD Fe/Cu(111) lasts up to 6 ML until the films transform from fcc to bcc structure. Similar to the PLD Fe/Cu(100) films, the PLD Fe/Cu(111) films have also an isotropic fcc structure. Below 3 ML the Fe/Cu(111) films possess the high-moment ferromagnetic phase and then become low-moment ferromagnetic when the thickness is higher than 3 ML. We have studied the lattice constant of the Fe films in both vertical and lateral directions, and found that they are closely correlated to the magnetic transitions of the Fe films. Part of the results has been briefly reported in Ref. 15.

II. EXPERIMENTAL ASPECTS

All the experiments were performed in a UHV multichamber system including an MBE chamber, a chamber for scanning tunneling microscopy (STM), a chamber for magneto-optical Kerr effect (MOKE), and an analysis chamber equipped with Auger electron spectroscopy (AES), low-energy electron diffraction (LEED) with intensity vs energy function (IV-LEED), and facilities for thin film growth by thermal deposition. Each individual chamber is linked by a central distribution chamber for sample transferring. The base pressure of each chamber is better than 5×10^{-11} mbar and never exceeds 2×10^{-10} mbar during evaporation. The preparation of the Cu(111) prior to deposition consists of cycles of Ar^+ sputtering and 20 min annealing (700 K) until a clean AES spectrum and a sharp $p(1\times1)$ LEED pattern have been obtained.

The PLD growth of Fe on Cu(111) was performed in the MBE chamber. A KrF excimer laser beam (248 nm wavelength, 34 ns pulse length, typical pulse energy 270–300 mJ and pulse repetition rate of 5 Hz) was focused onto an Fe target (4*N* purity). To avoid the droplet formation the laser energy is chosen very close to the ablation threshold while striking on a rotating target, and the substrate is placed approximately 100 mm away from the target. The instantaneous deposition rate, i.e., the deposition rate during each laser pulse, is of the order of 10^6 ML/min. Between two subsequent laser pulses there is a long break (on the order of a tenth of a second) resulting in an average deposition rate comparable to that of the thermal deposition. The film thickness was monitored by reflection high-energy electron-diffraction (RHEED) oscillations and cross-checked afterwards by AES and STM. During deposition the sample was kept at 220 K to minimize the interdiffusion process between Fe and Cu. After film preparation the sample is transferred to the MOKE chamber allowing polar and longitudinal MOKE characterization. There, the measuring temperature can be varied from 40 to 500 K. After the magnetic characterization the sample is moved to other chambers for further structural investigation. The morphology is deduced from the room-temperature STM and the crystalline structure was analyzed by LEED, IV-LEED, and RHEED.

For comparison, we have also prepared Fe films on the same Cu(111) substrate at the same substrate temperature (220 K) by thermal deposition. The deposition rate was typically about 0.2 ML/min. Due to the lack of RHEED oscillations caused by the three-dimensional (3D) growth, a quartz monitor which has been calibrated by STM was used to control the thickness of the TD Fe/Cu(111) films.

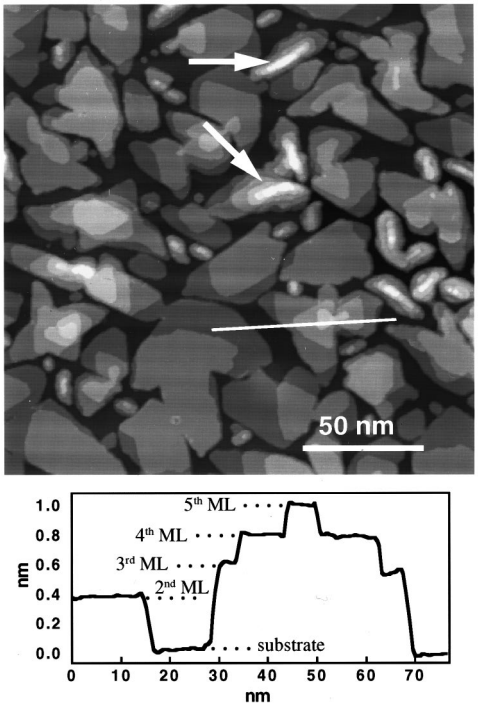

FIG. 1. STM topography image of a 2 ML TD Fe/Cu(111) film. The marked line profile is shown below the image, which clearly indicates that there are five layers exposed on the surface. Some of the bcc ridgelike structures are indicated by white arrows.

III. RESULTS

A. Improved morphology and structure of the PLD films

Thermally grown Fe/Cu(111) films have a 3D island morphology. Figure 1 shows the typical STM topography image of a 2 ML TD film grown at 220 K. The marked line profile, shown below the STM image, indicates that there are five layers exposed on the surface, ranging from the bare substrate to the fifth deposit layer. A considerable amount of ridgelike structures, some of which are indicated by white arrows, are also clearly visible in the image. These ridgelike structures are known to be bcc(110) domains with a Kurdjumov-Sachs (KS) orientation.[10] Apparently for the TD films a fcc→bcc phase transformation starts to proceed at very early stages of growth.

The bcc formation has also been observed as a major obstacle for improving the TD growth towards layer-by-layer. In the TD process, varying substrate temperature is a common way to control the growth mode. However, for this particular system Fe/Cu(111), there is only a rather narrow temperature window, i.e., from 80 to 300 K, which can be used in the deposition process. This is because that at higher temperatures the system suffers significant interdiffusion while at lower temperatures the films were observed to grow directly in the bcc phase. In the mentioned temperature window, we have found no suitable temperature for the film to grow layer-by-layer at the typical TD deposition rate (on the order of 1 ML/min).

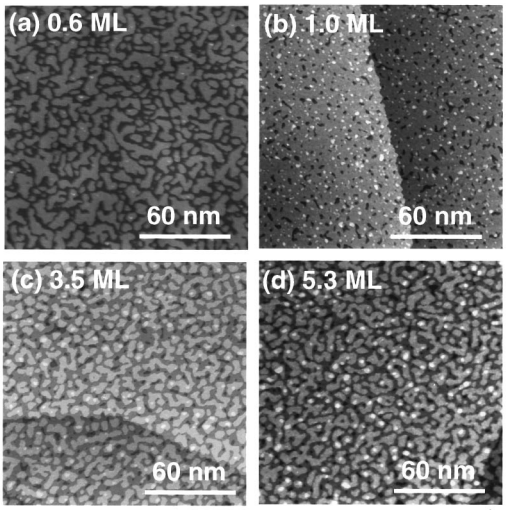

FIG. 2. STM topography images of 0.6 ML (a), 1.0 ML (b), 3.5 ML (c), and 5.3 ML (d), PLD grown Fe/Cu(111) films. Compared to the TD films, the PLD film morphology shows significant improvement towards layer-by-layer growth. Note that no bcc-ridge structures can be observed even in the 5.3 ML image.

To significantly increase the deposition rate in the TD process is practically difficult. The PLD technique, as mentioned, offers an easy way to increase the deposition rate by several orders of magnitude. Under such a high-deposition rate, the growth of Fe on Cu(111) has been dramatically modified to be layer-by-layer like. Figure 2 shows a series of STM images of the PLD grown Fe/Cu(111) films at various thickness. It is immediately clear that the films grow in a near layer-by-layer mode, which is in stark contrast to the TD film shown in Fig. 1. The layer filling at each thickness can be calculated directly from the histogram of the STM morphology. Figure 3 shows the layer filling as a function of total coverage. Up to 5 ML, no more than three layers are exposed on the surface at any thickness. For example, at 1 ML more than 90% of the substrate has been filled by the first layer, and at a thickness of 4 ML, the fourth layer covers about 80% of the total area while the fifth layer islands are within 20% of the total area.

Another remarkable feature of the PLD films in Fig. 2 is the absence of bcc ridgelike structures which are clearly visible in the TD film (Fig. 1) even at early stages of growth. In fact, as shown in Fig. 4, at any given thickness above 3 ML the TD film morphology is already dominated by the bcc domains oriented along the $\langle 011 \rangle$ directions. In this respect, the fcc structure of the PLD films is more stable than that of the TD films with respect to the fcc→bcc phase transformation.

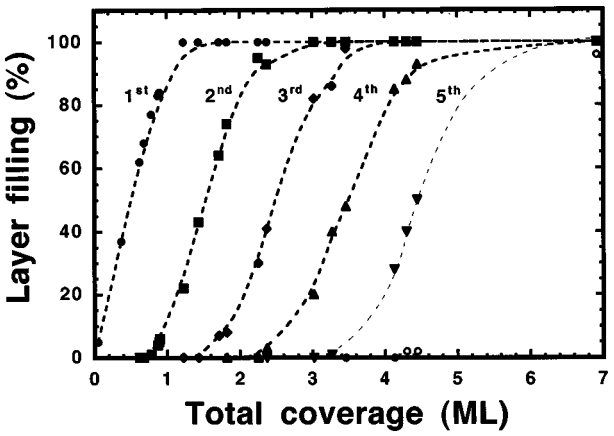

FIG. 3. Layer filling as a function of the total coverage of the PLD Fe/Cu(111) film. This plot provides the quantitative information of the growth mode.

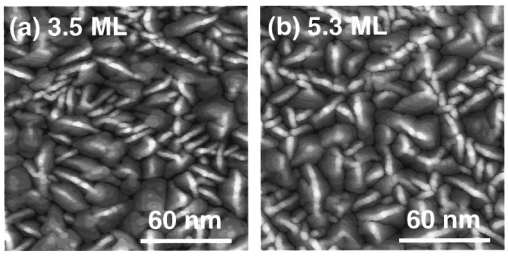

FIG. 4. STM topography images of 3.5 ML (a) and 5.3 ML (b) TD Fe/Cu(111) films. The bcc ridgelike structures become already significant at 3.5 ML, and completely dominant at 5.3 ML.

The details of the fcc→bcc transformation mechanism are better clarified by LEED and IV-LEED studies. Figure 5 shows the LEED patterns taken at 90 eV for both TD (left column) and PLD (right column) films. The fcc phase for both films is characterized by a clear $p(1\times1)$ LEED diagram. For the TD films thicker than 3 ML, the LEED diagram becomes more complicated illustrating the growth of Fe bcc(110) along the KS orientation. In this epitaxial relationship the dense-packed rows of the bcc(110) ($\langle \bar{1}11 \rangle$) are parallel to the dense-packed row of the fcc(111) ($\langle 110 \rangle$). Due to the symmetries there are six energetically equivalent domains which appear as the elongated islands along the $\langle 011 \rangle$ substrate directions in the STM pictures (Fig. 4). These domains result in six satellite spots around each substrate spot

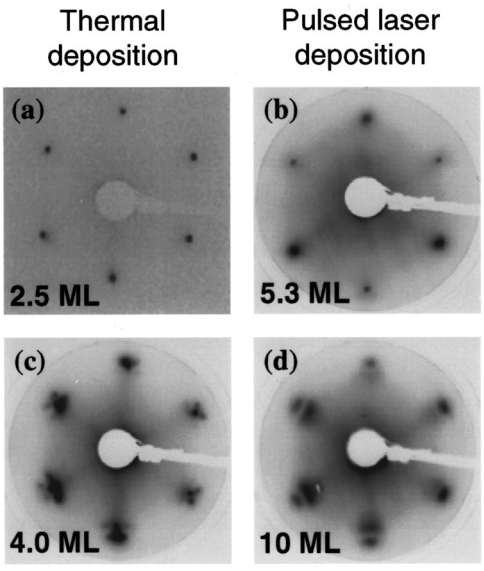

FIG. 5. LEED patterns of TD (left column) and PLD (right column) Fe/Cu(111) films taken at 90 eV. For the TD film, the LEED pattern is that of $p(1\times1)$ below 3 ML. Above 3 ML, patterns of Kurdjumov-Sachs oriented bcc(110) structure have been observed. For the PLD films, the fcc to bcc transformation occurs at about 6 ML.

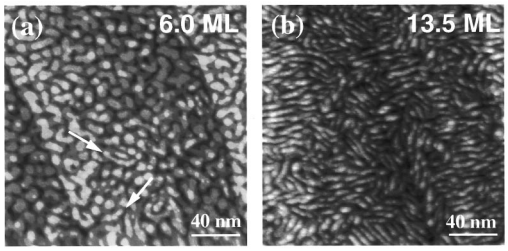

FIG. 6. Surface morphology of the PLD films at 6.0 ML (a) and 13.5 ML (b). Note that the bcc precipitates start to appear in the 6.0 ML film (indicated by the white arrows), and become dominant in the 13.5 ML film. The size of the bcc precipitates in the PLD films is clearly smaller than those of the TD films (e.g., see Fig. 4).

in the LEED pattern (in fact only five satellites can be seen because two of them always merge with each other).

In the PLD case the $p(1\times1)$ pattern remains sharp until the fcc→bcc transformation at 6 ML which is consistent with Fig. 2 as no signs of bcc structures are visible in the PLD films below 6 ML. At higher thickness, the fcc to bcc phase transformation starts to proceed rapidly. As an example, we show the LEED pattern of a 10 ML PLD film in Fig. 5(d). Despite that the diffraction spots are rather diffuse, the LEED pattern reflects the KS oriented bcc(110) structure. STM indicates that the diffuse LEED spots in Fig. 5(d) are a direct consequence of the formation of the bcc phase. Figure 6 shows the STM morphology of PLD films at 6.0 ML in (a) and 13.5 ML in (b). The bcc structures, indicated by the white arrows, start to appear at 6.0 ML and become apparently dominant at 13.5 ML. The bcc precipitates in the PLD films are smaller than those in the TD films (see Fig. 4). Figure 6(b) clearly shows that the size of the bcc precipitates is of the order of 10 nm or less, which explains why the corresponding LEED spots are so diffuse.

The fcc→bcc phase transformation as well as other structural information such as the evolution of the lattice parameters are further studied by IV-/LEED and RHEED. The IV-LEED curves are obtained by recording the intensity of the (00) LEED beam as a function of the electron energy. To measure the (00) spot the primary electron beam is tilted approximately 6° from the sample normal. The curves obtained from the PLD films at various thickness are shown in Fig. 7. The curves of the films in the fcc regime (<6 ML) closely resemble the curve recorded from the clean Cu(111) substrate suggesting that no clear tetragonal distorsion exists in the PLD films which would otherwise lead to a clear peak shift or even the appearance of a second family of peaks. Only above 6 ML a second family of peaks appears (solid lines in Fig. 7) with a slight shift to the higher energies as compared to the fcc peaks (dotted lines in Fig. 7). With the knowledge of the LEED and STM studies, we conclude that the peak shift is caused by the fcc to bcc phase transformation.

In order to obtain more quantitative data we apply a simple kinematical model on these curves. This model does not allow analyzing each interlayer distance but rather yields the average interlayer distance with some systematical error due to the simplification of the model. By proceeding this way for both TD and PLD films, the variation of the average interlayer distance with the film thickness is obtained (Fig. 8). The fcc to bcc phase transformation appears clearly with the drop of the interlayer distance at approximately 3 ML for the TD films and at 6 ML for PLD films. The drop of the kinematically calculated average interlayer distance at the transition thickness reflects the fact that the interlayer distance of the fcc Cu(111) planes (2.08 ± 0.01 Å) is slightly higher than that of the bcc Fe(110) structure (2.04 ± 0.01 Å).

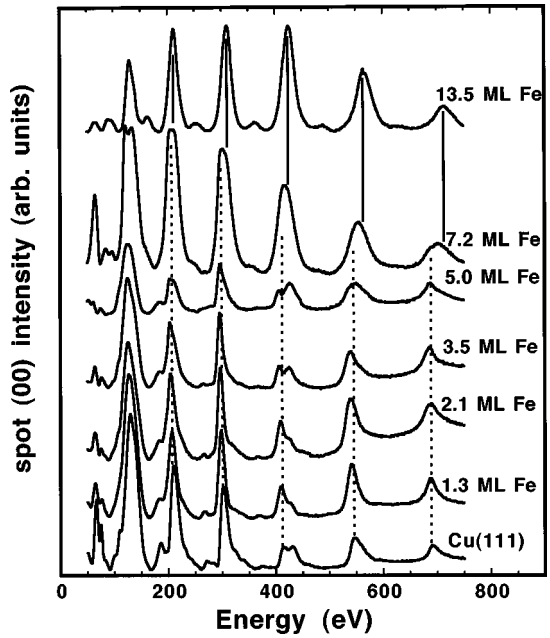

FIG. 7. IV-LEED curves of the (00) beam of the PLD Fe/Cu(111) films at various film thickness. The dotted lines mark the fcc peak positions of the copper substrate. The solid lines indicate the bcc peak positions of a 13.5 ML film which has been completely transformed into the bcc structure.

The in-plane lattice parameter is determined from RHEED experiments. In the experiment we store the

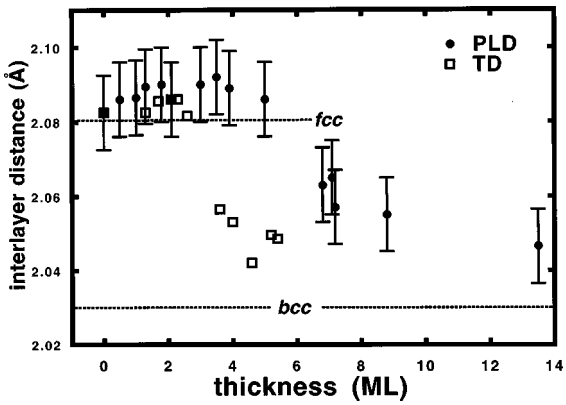

FIG. 8. Calculated average interlayer distance of the PLD (full circles) and TD (open squares) Fe/Cu(111) films. The arrows indicates the values for the bulk fcc Cu(111) and bulk bcc Fe(110). The decrease of the interlayer distance is caused by the fcc-bcc structural phase transformation, which occurs at 3 ML for the TD film and at 6 ML for the PLD film. In the fcc region, the interlayer distance of the TD and the PLD films are virtually the same. Note that the calculated values of the TD and PLD films have a similar error bar, though it is not indicated for the TD films in order to get a clear view of the error bars of the PLD data.

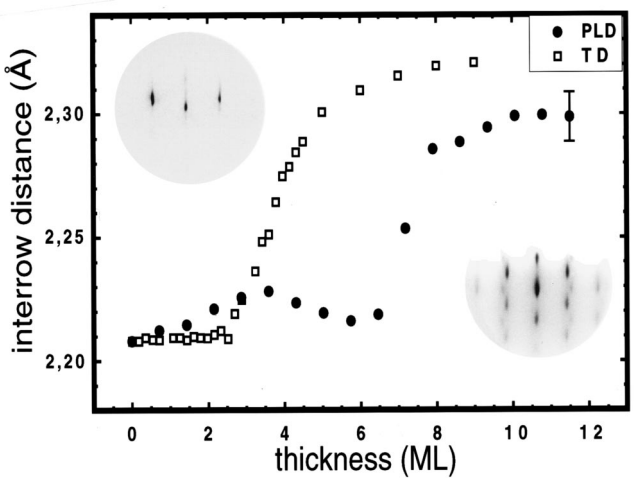

FIG. 9. Interrow distance between two neighboring dense rows ($\langle 110 \rangle$) as a function of the thickness of the PLD (full circles) and TD (open squares) Fe/Cu(111) films. The inset pictures show the RHEED patterns of fcc(111) in the upper left and bcc (110) in the lower right. The rapid increase of the in-plane lattice constant for both TD (at 3 ML) and PLD (at 6 ML) are due to the bcc formation. In the fcc regime, the in-plane lattice constant of the PLD films appears to be slightly larger than that of the TD films.

RHEED patterns at regular time steps during a high-coverage deposition experiment. The corresponding thickness for each RHEED pattern is deduced from the final coverage, the total evaporation time and the time step. Line profiles across the maxima of the (01) and $(0\overline{1})$ streaks were then made for each pattern (typical RHEED patterns for the fcc and bcc Fe are displayed as inset pictures in Fig. 9). The distance between these two maxima, i.e., the in-plane lattice parameters in reciprocal space, was determined using a Gaussian fit in order to find the precise peak positions. The corresponding in-plane lattice constants, i.e., the distance between two neighboring dense rows ($\langle 110 \rangle$), of the Fe films can then be calculated by comparing the reciprocal-lattice distance between the Fe films and the Cu substrate, assuming that the value for the Cu surface layers equals to that of the bulk (2.21 Å). By this way we can plot the variation of the in-plane parameter as a function of the coverage as shown in Fig. 9. In accordance with the LEED studies, Fig. 9 shows that the fcc to bcc transformation appears clearly for both PLD and TD around 6 and 3 ML, respectively, as indicated by the rapid increase of the lattice parameter (the distance between the $\langle 110 \rangle$ dense rows of bulk bcc Fe(110) is 2.34 Å). Before the fcc→bcc phase transformation occurs, the PLD films appear to have a slightly larger in-plane lattice constant compared to the TD films. This fact, as will be discussed later in the paper, has a close correlation to the magnetism of the PLD Fe films.

B. Long-range order and enhanced magnetic moment of the PLD films

Having demonstrated the improvement of the growth and structure with the PLD it is now interesting to compare the magnetic properties of the thermally deposited and the pulsed-laser deposited Fe/Cu(111) films. We first concentrate on the anisotropy behavior of the films. Figure 10 shows the

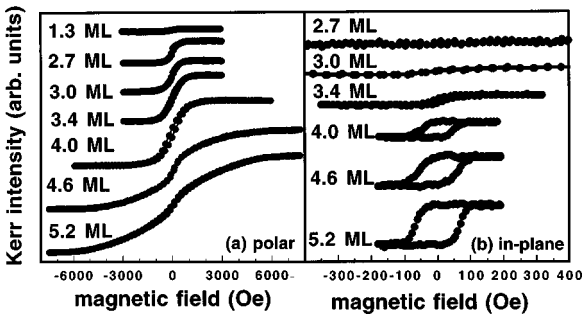

FIG. 10. Measured Kerr loops of TD Fe/Cu(111) film at 150 K. (a) polar loops; (b) longitudinal loops. The longitudinal loops start to appear at a thickness of about 3 ML, at which the bcc structure starts to form.

polar and longitudinal Kerr hysteresis loops of the TD Fe/Cu(111) films in the left and right column, respectively. Below 3 ML the measured polar loops are all with full saturation while no longitudinal loops can be detected, indicating that the easy magnetization axis is perpendicular to the film surface. Note that the polar curves of the films below 3 ML show little remanence at the measured temperature of 150 K. We will show later that the TD films (<3 ML) exhibit a sizable remanence in the perpendicular direction only at considerably lower temperatures. At thickness above 3 ML, the TD films undergo a clear spin reorientation from perpendicular to in-plane, as evidenced by the appearance of the in-plane Kerr loops with nearly full remanence as well as the polar hard-axis loops.

The PLD films have a perpendicular easy axis below 2 ML. As an example, Fig. 11 displays the polar Kerr loops of a 1.6 ML PLD film measured at various temperatures. For curves measured well below the Curie temperature (220 K), they all show a well-defined rectangular shape with full remanence. No in-plane Kerr loops have been observed even when an external field of 0.8 T was applied. Above 2 ML,

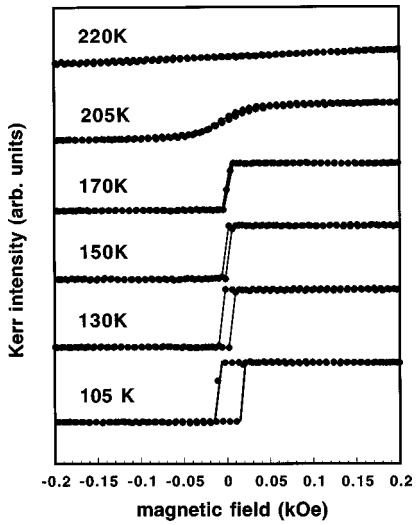

FIG. 11. Polar Kerr hysteresis loops of a 1.6 ML PLD Fe/Cu(111) film recorded at various temperatures. At low temperatures the loops show a well-defined rectangular shape with full remanence, indicating the easy magnetization axis is perpendicular to the surface.

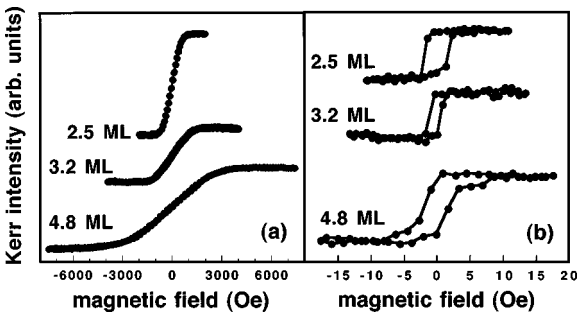

FIG. 12. Measured Kerr loops of PLD Fe/Cu(111) films at 150 K. (a) polar loops; (b) longitudinal loops. Above 2 ML, the polar loops become hard-axis like while in-plane loops start to be measurable.

the easy magnetization axis of the PLD films switches from perpendicular to in-plane. Figure 12 shows the polar and longitudinal Kerr loops in the left and right column, respectively. It is immediately clear that the PLD films also experience a spin reorientation from perpendicular to in-plane but at a slightly smaller critical thickness than that of the TD films.

Although both TD (<3 ML) and PLD (<2 ML) have perpendicular easy magnetization axis at low thickness, their Kerr loops show remarkably different characteristic features. As already shown in Figs. 10 and 11, the TD films show an S-shaped polar loop with little remanence, while the PLD films show a well-defined rectangular loop with full remanence. The rather small remanent magnetization of the TD films in the direction of the easy magnetization axis is an indication that the films do not have a true long-range ferromagnetic order. This is better characterized by time-dependent remanent magnetization (M_r) measurement. Figure 13 shows the magnetization vs time curves of a 1.6 ML TD film in the lower panel and of a 1.6 ML PLD film in the upper panel. Both curves were recorded at 130 K. The inset pictures are the correspondingly measured polar Kerr loops taken at the same temperature. The zero level of the Kerr signal corresponds to the one recorded after the sample demagnetization. At the time scale zero, an external field of about 6 kOe was switched on in the direction perpendicular to the film surface. The Kerr signals of both TD and PLD films rise rapidly to reach the saturation level. Twenty-five seconds after being switched on, the external field was removed as indicated by the dashed line in Fig. 13. For the PLD film, the remanent magnetization keeps constant without showing any signs of decaying with time. This is a clear sign of a true long-ranged ferromagnetic order in the PLD Fe film. For the TD film, however, the remanent magnetization clearly decays with time. Such a decay of the remanent magnetization could be obtained by either nucleation and growth of domains with reversed direction, or a superparamagnetic behavior of the films. Considering the island morphology of the TD films, we believe that the former may occur in the large islands, while the latter occurs in the islands with smaller size.

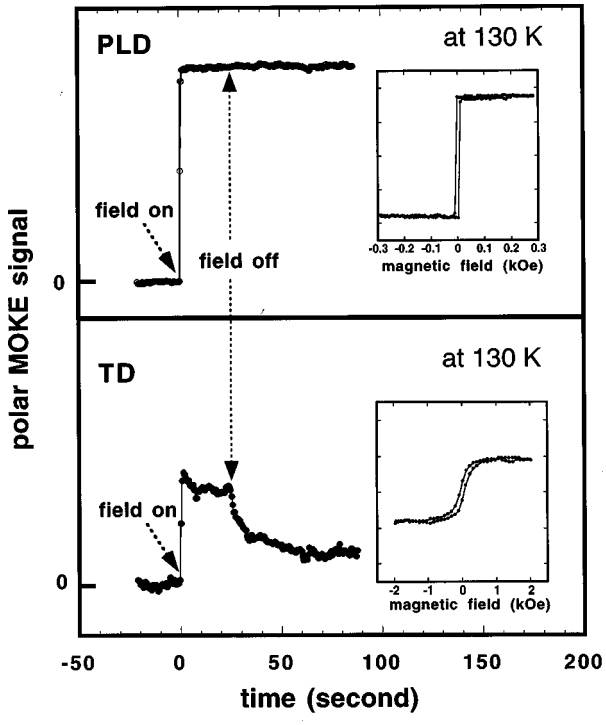

FIG. 13. Time-dependent magnetization of a 1.6 ML PLD (upper panel) and a 1.6 ML TD (lower panel). Fe/Cu(111) films. The curves are recorded at 130 K in the polar geometry. The inset pictures are the corresponding polar hysteresis loops. After the removal of the external field (0.6 T), the remanent magnetization of the PLD film stays constant while the remanent magnetization of the TD film decays with time.

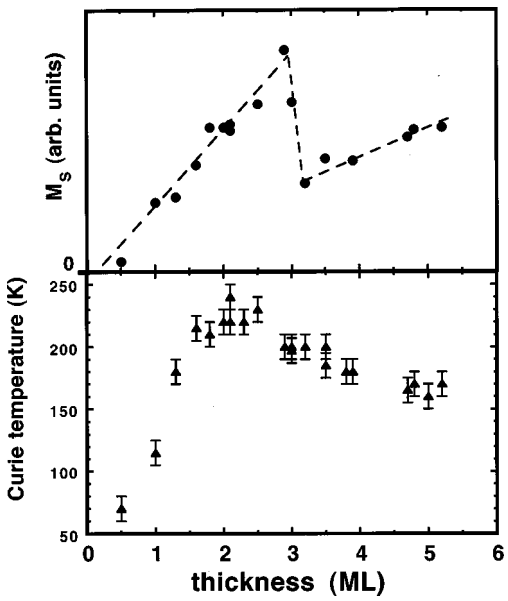

FIG. 14. Saturation magnetization along the surface normal (upper panel) and Curie temperature (lower panel) as a function of the thickness of the PLD films. M_s increases linearly with thickness reaching its maximum at about 3 ML, and then drops to a smaller value. At higher thickness M_s again linearly increases but with a smaller slope. The Curie temperature reaches a maximum at 2 ML, and then gradually decreases with increasing thickness.

Because the PLD films show a promising long-range ferromagnetic order with a perpendicular magnetization, their magnetic properties deserve further investigation. Figure 14 shows the saturation magnetization (M_s, upper panel) and the Curie temperature (T_c, lower panel) as a function of

thickness of the PLD films. Note that all the M_s values were determined from the saturated polar Kerr loops irrespective whether the easy magnetization axis is in-plane or perpendicular. M_s initially increases linearly with thickness reaching its maximum at about 3 ML. Above 3 ML M_s falls rapidly to about 40% of the M_s of the 3 ML film. With further increasing thickness, M_s again increases linearly with thickness although the slope now is significantly smaller than that of the initial increase. Despite the sudden drop of the magnetization, the whole PLD film is still in a ferromagnetic phase above 3 ML since a backward linear extrapolation of M_s above 3 ML crosses the origin. However, the magnetic moment of the PLD films at higher thickness (>3 ML) is clearly smaller than that of the thinner films (<3 ML) as evidenced by the distinctly smaller increasing slope of the saturation magnetization. This implies that the PLD films have experienced a magnetic phase transition from a high-moment ferromagnetic phase to a low-moment ferromagnetic phase at a thickness of about 3 ML.

With increasing thickness, the magnetic phase transformation of the PLD films is accompanied by another magnetic effect: the nonmonotonic behavior of T_c with increasing thickness, as shown in the lower panel of Fig. 14. The T_c value was determined by the temperature where the saturation magnetization disappears. This is reasonable as the saturation field of the PLD films is rather small (of the order of 10 Oe) due to the high quality of the morphology and structure. After a linear increase up to 250 K at 2 ML, the Curie temperature of the PLD films starts to gradually decrease reaching 170 K at 6 ML, above which the fcc to bcc phase transformation starts to proceed. The transformed bcc films have a Curie temperature well above 400 K which was intentionally not checked in order to avoid interdiffusion. For the TD films (<3 ML), as mentioned above, there exists no true long-range ferromagnetic order and thus no Curie temperature. There is, however, evidence that the critical temperature of the individual superparamagnetic spin blocks is above 300 K as the films can still be saturated by a moderate external field of several thousand Oe above room temperature. Again, because of the interdiffusion problem, we have made no efforts to determine the critical temperature of the individual spin blocks.

The magnetic moment of the PLD films can be estimated from the measured Kerr signals. While the Kerr signal does not give an absolute value of the magnetic moment, in this particular Fe/Cu(111) system it is possible to estimate the magnetic moment of the fcc Fe films from the Kerr signal measured from the transformed bcc Fe films. For this we make two basic assumptions: (1) the Kerr intensity is proportional to the magnetization of both fcc and bcc films; (2) the transformed bcc Fe films possess the magnetic moment of the bulk α-Fe, i.e., $2.2\mu_B$. In our previous work we have verified that the first assumption is true,[9] while the second assumption appears to be also reasonable since the magnetic moment of bcc Fe is much less sensitive to the change of the lattice parameters as compared to that of the fcc Fe.

To avoid any possible complications of the normalization between longitudinal and polar Kerr signals, we will compare the saturated polar Kerr signals only, no matter whether the easy magnetization axis lies perpendicular or parallel to the surface. Because the maximum magnetic field in our system (0.8 T) turns out to be enough to saturate bcc Fe films thinner than 5 ML in the perpendicular direction (hard axis), we will use the bcc TD films (between 3 and 5 ML) as our reference for the determination of the magnetic moment of both TD fcc (<3 ML) and PLD fcc (<6 ML) Fe films. Figure 15 shows the saturated polar Kerr signal of the PLD (full circles) and TD (open squares) films as a function of the thickness. It is immediately clear that the increasing slope of the fcc TD films (<3 ML) is more than four times smaller than that of the bcc TD films (>3 ML), implying that the magnetic moment of the fcc TD films is about four times smaller than that of the bcc Fe ($2.2\mu_B$), i.e., about $0.5\mu_B$. For the high-moment fcc PLD films (<3 ML), their magnetic moment should be close to $2.2\mu_B$, because the increasing slope, and thus the magnetic moment, is comparable to that of the bcc TD films. With similar arguments, one can determine the magnetic moment of the low-moment fcc PLD films (3–6 ML) to be about $0.8\mu_B$.

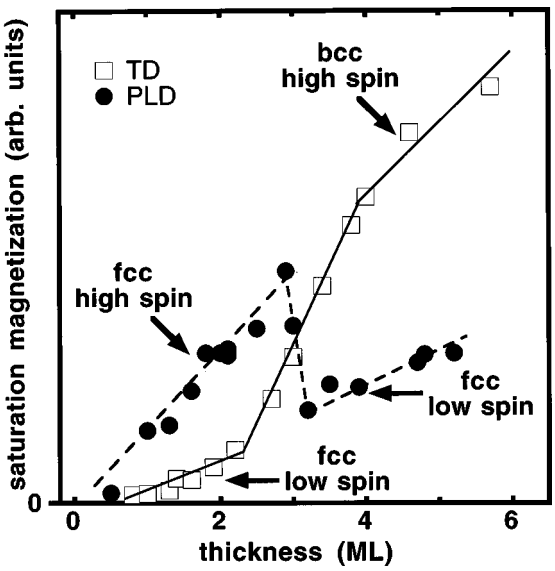

FIG. 15. Saturation magnetization as a function of the thickness of the thermally (open squares) and pulsed-laser deposited (full circles) Fe/Cu(111) films. The thermal films have low moment below 2 ML. Between 2 and 4 ML, their total moment increases quickly, in accordance with the rapid progress of the fcc→bcc phase transformation in this region. In the bcc region (>4 ML), the moment of the films is nearly four times higher than the expected values based on a linear extrapolation of M_s from the fcc films (<2 ML). For the pulsed-laser deposited films, the magnetization initially increases linearly at a rate of about $2\mu_B$ per atom per monolayer reaching the maximum at about 3 ML. Above 3 ML, the moment first falls down to about 40% of that of the 3 ML film, and then linearly increases with a slope of about $0.7\mu_B$ per atom per monolayer. Note that at a given nominal thickness below 3 ML, the moment of the pulsed-laser deposited films is strongly enhanced, up to a factor of 4 to 5, as compared to that of the thermal films.

IV. DISCUSSION

A. Morphology and structure

The STM experiments clearly show that the PLD Fe/Cu(111) films grow layer-by-layer up to the critical thickness of the fcc→bcc phase transformation (6 ML). Layer-by-layer

growth is highly desirable because it leads to a lower surface roughness which is important to create sharp interfaces in terms of growing magnetic multilayers, and it also helps the understanding of the correlation between structure and magnetism in a more straightforward way. The further advantage of using PLD to achieve this growth mode is that there are no other materials such as surfactants involved, which could complicate the situation as the issue may be raised whether the measured magnetic properties stand for the intrinsic magnetism of the system or not.

Because of the great usefulness of the PLD technique, it is important to understand the PLD growth mechanism which apparently supports a two-dimensional growth. We believe that the high nucleation density plays a key role in the final growth mode of the PLD films. The high nucleation density, however, is a result of the extremely high instantaneous deposition rate rather than the average deposition rate of the PLD which is in the same order of magnitude of that of the TD. In the following, we discuss the different growth process of PLD and TD.

In case of PLD the laser beam pulse of several ten nanoseconds duration, evaporates surface atoms of the target. As the laser energy is at the ablation threshold, the target atoms are mostly set free by thermal process at the surface while some nonthermal (bond breaking) processes are also involved. The evaporating atoms then adsorb the laser light resulting in the partial ionization of the evaporating atoms and, thus, in the formation of a plasma, which expands away from the target. This laser-generated plasma plume has a lifetime of approximately 100 ns. The liberated atoms and ions have a rather wide nonthermal energy distribution with a peak at about 1 eV (the tail of the ion energy distribution may reach up to several 10 eV with low intensity, that of the neutrals is largely unknown). If we take the flight distance and the energy spread into account, this means that within 0.1 to 1 μs after the laser shot the Fe atoms from the target arrive at the sample. Then a long pause follows, in the order of 10^5 μs given by the laser pulse repetition frequency (5 Hz in our experiment). With our setup the deposition rate per shot is 10^{-2}–10^{-3} ML, or at our repetition frequency around 1 ML within a few minutes. This explains the difference between a high instantaneous deposition rate (approximately 10^4 ML/s during the duration time of the plasma plume, i.e., approximately 1 μs) and the low average deposition rate of the order of only 1 ML per 100 s. It is known that the number of nuclei scales with $(F/D)^{\chi}$, where F is the flux and D is the diffusion coefficient (the exponent depends on the types of nucleation process ranging from 1/3 to 1/2).[16] So during one laser shot the high evaporation rate of the laser and the small critical nucleus for metals on metals (two atoms mostly form a stable nucleus) lead to a high nucleation density. This scenario looks almost ''frozen-in'' until the next laser shot occurs. In reality, the nuclei are still mobile but at much lower speed. Therefore some Ostwald ripening goes on, i.e., the agglomeration of small nuclei to larger islands, but the relatively high nucleation density persists. After the next laser is triggered, the whole scene comes into motion again, with many ''singles'' diffusing around, but after a short time meeting ''slow'' nucleation centers to reach the dock. In this way a complete monolayer is slowly filled (after approximately 100 s in our example).

Now we consider the TD deposition at the *same* average deposition rate but with continuous deposition. Because of the very low instantaneous deposition rate, on the time scale of 10 μs there are much less Fe atoms arriving at the sample surface as compared to the PLD case. This means that the probability of forming critical nuclei on short distance is much reduced compared to PLD. In other words, each single Fe atom has time to wander a long path on the crystal before meeting a partner. This results in a large distance between individual nucleation centers, i.e., in a low nucleation density. This low nucleation density in turn may favor the tendency of the system to grow in multilayer or island formation modes, which has been clearly evidenced by STM images of the TD Fe/Cu(111) films.

Yet some disadvantages for the PLD have been reported in the literature, in particular regarding the droplet problem.[17] We have, however, successfully avoided the droplet problem by depositing films at a large substrate-target distance as well as working at low laser power which is just slightly above the ablation threshold. This has been proved by both STM and even large scale scanning electron microscopy (SEM). Nevertheless, as already mentioned, a few parts of the incident atoms have high kinetic energies, larger than the thermal kinetic energy of atoms in the TD techniques ($\ll$1 eV). These kinds of atoms can produce some defects on the surface, which might further favor the two-dimensional growth in the same way as the sputtering deposition process.[18]

In addition to the improvement of the surface morphology, the PLD grown Fe/Cu(111) films have a significantly more stable fcc phase which transforms to bcc structure at a thickness much higher than that of the TD films. The thermally grown Fe films, according to our STM and LEED studies, show a fcc-like structure only up to 3 ML above which the film transforms into the bcc(110) structure with Kurdjumov-Sachs orientation. Our results agree well with previous findings[8] on TD Fe/Cu(111) films except a certain difference of the critical thickness of the fcc→bcc transformation. We should mention that this critical thickness can vary from one study to the other mainly because of the difficulty to estimate the film thickness of a 3D growth of the TD films, not to mention the possibly different experimental conditions. In the present work, since the PLD films and the TD films were grown in the same UHV system at the same substrate temperature, the fact that the fcc phase of the PLD films is more stable with respect to the fcc to bcc phase transformation compared to the TD films has been proven unambiguously.

The reason why the PLD grown Fe/Cu(111) films have a more stable fcc phase compared to the TD films needs to be further discussed. For simplification, we assume that the actual critical thickness of fcc→bcc transformation is 6 ML in both PLD and TD films. For the TD films with 3D island morphology, at a nominal thickness of about 3 ML (see Fig. 4) most of the islands contain six layers or more leaving wide gaps in between the islands. Because the local thickness of the islands has reached the critical thickness, it is understandable that films start to transform into the bcc phase even though the nominal thickness is only 3 ML. By the same argument, it is straightforward to understand that the layer-by-layer grown PLD films will reach the critical

thickness locally only when the nominal thickness is six monolayers. Certainly some other governing factors of the fcc→bcc phase transformation, such as local stress in the film,[19] might also be different in the two types of films due to the growth mode, which results in a overall delayed structural phase transformation in the PLD films.

For understanding the magnetic properties, it is important to compare the lattice parameters of the PLD and TD films according to our IV-LEED and RHEED results. Our kinematical approximation allows us only to obtain an average interlayer distance with no real sensitivity to each plane. Yet within this limitation we can compare the average interlayer distance between the PLD and TD films. The calculated values in Fig. 8 clearly indicate that there is no distinct difference between the PLD and TD films in terms of the average interlayer distance. A better accuracy for the interlayer distances would need a dynamical LEED calculation which is currently in progress.

For the in-plane lattice parameter we use RHEED, since the less sensitive LEED pattern does not indicate any difference between the in-plane lattice constants of the PLD and TD films. According to the RHEED data, the TD films appear to adopt the lattice constant of the Cu substrate in the fcc regime (<3 ML). When the films transform to bcc phase, the in-plane lattice constant accordingly increases as shown in Fig. 9. The PLD films, despite of having the similar interlayer distance as the TD films, show a slightly larger in-plane lattice constant than the TD films at a thickness below 3 ML. It is not immediately clear whether the PLD Fe films have the same in-plane lattice constant at all thicknesses below 3 ML, even though Fig. 9 shows that the measured in-plane lattice constant from RHEED data appears to increase with thickness only reaching the maximum at 3 ML. This is because at very low thickness the RHEED data of the Fe films is likely affected by the underlying substrate, whose influence only becomes negligible when the films are thicker than 2 ML. For this reason, while the measured values in Fig. 9 might underestimate the real in-plane lattice constant of the PLD Fe films below 3 ML, it is clear that the in-plane lattice constant does become smaller when the thickness is higher than 3 ML.

Combining the information of the IV-LEED and RHEED data, we conclude that below 3 ML the atomic volume of the PLD fcc Fe/Cu(111) films is slightly larger than that of the TD fcc Fe films as well as that of the copper substrate. Above 3 ML, the atomic volume of the PLD fcc films becomes smaller than that of the thinner films. The variation of the atomic volume of the PLD Fe/Cu(111) films appears to be closely correlated with their magnetic moment, which will be discussed below.

B. Magnetic properties

We start our discussion with the magnetic moment of the PLD Fe/Cu(111) films in the fcc thickness regime (<6 ML). Fcc Fe is well known for its rich magnetic structure and their strong dependence on the lattice constant. With increasing lattice constant, the magnetic phase of fcc Fe can be nonmagnetic, antiferromagnetic, low-moment ferromagnetic, and high-moment ferromagnetic. While generally a larger lattice constant favors a larger magnetic moment as well as ferromagnetic coupling, in a certain crossover regime such as the lattice constant of copper which is in between that of the antiferromagnetic and the ferromagnetic phase, the energy difference between different magnetic phases is often very small. As a result, not surprisingly the Fe/Cu system often shows rather complex magnetic phases depending on the film thickness. In the particular PLD Fe/Cu(111) system, a clear magnetic phase transformation from high-moment ferromagnetic to low-moment ferromagnetic has been observed at a thickness of about 3 ML. This magnetic phase transformation appears to be closely correlated with the change of the lattice parameters: The in-plane lattice constant of the films below 3 ML is slightly larger than that of films above 3 ML. As mentioned, at a lattice constant in a crossover regime, even the slightest change of the lattice constant could result in a magnetic phase transition. This might explain that the PLD films become low-moment ferromagnetic above 3 ML.

For the TD films, it is not surprising that they have a low magnetic moment because their in-plane lattice constant is consistently smaller than that of the PLD films. Such a low magnetic moment has also been observed in TD Fe/Cu(111) films capped by copper overlayers[9] and TD Fe films on a stepped Cu(111) substrate.[10] The low magnetic moment of the TD Fe films, however, has to be distinguished from the low moment of the PLD Fe films. This is because the TD films do not exhibit a real long-range ferromagnetic order as shown by the time-dependent magnetization measurement (Fig. 13). The lack of the long-range order is a direct result of the 3D island morphology: the rather isolated islands lead to a short-range order within each island but overall the system has no real long-ranged order. Such a short-range order in fact has already been observed by Rau *et al.* in their electron capture spectroscopy experiment.[20] For the PLD films, the well-improved morphology, as expected, leads to a real long-range ferromagnetic order as shown in Fig. 13.

We now turn to discuss the anisotropy behavior of the PLD and TD Fe/Cu(111) films. Both types of films, at low thickness, exhibit perpendicular anisotropy which is apparently large enough to overcome the in-plane shape anisotropy since the easy magnetization axis is perpendicular to the film surface. With increasing thickness, both PLD and TD films undergo a spin reorientation from perpendicular to in-plane. For the TD Fe films, the switching of the easy magnetization axis occurs at about the same thickness as the fcc→bcc phase transformation. This is not just a mere coincidence because the transformed bcc (110) surface has an additional twofold in-plane anisotropy which adds to the in-plane shape anisotropy in competition against the perpendicular surface anisotropy. As a result, the overall easy magnetization axis switches to in-plane after the formation of the bcc structure at about 3 ML. Such spin-reorientation has also been observed in the Fe/Cu(100) system where a similar mechanism holds.[7]

In the case of the PLD films, the spin-reorientation purely results from the competition between the in-plane shape anisotropy and the perpendicular surface anisotropy. No associated structural change has been observed by our LEED and RHEED investigations. Instead, this is simply a thickness effect: with increasing thickness, the contribution of the surface anisotropy remains unchanged and that of the shape anisotropy increases. There have also been discussions that

the balance between the surface and the shape anisotropy could be modified by the surface roughness,[21] but this does not apply to the PLD films, which have a constant surface roughness throughout the thickness region where the films have a fcc structure due to its layer-by-layer growth.

Our experimental results seem to contradict some of the theoretical calculations[22,23] which predict an in-plane anisotropy for the monolayer Fe/Cu(111) film. At this stage the origin of the discrepancy between the theory and the experiment is not clear. This is particularly puzzling in the case of the PLD films since the morphology and the structure of the PLD films resemble as closely as possible the theoretical assumption of the monolayer film being flat and free of distortion. There is, however, one calculation made by Bruno predicting a small out-of-plane anisotropy of about -0.6 meV/atom.[24] The order of magnitude of the out-of-plane anisotropy (surface anisotropy in this case) of the PLD Fe/Cu(111) films can be estimated according to a simple phenomenological equation describing the balance between the surface anisotropy (K_s) and shape anisotropy (K_{shape}), i.e., $-2K_s = d_c * K_{\text{shape}}$, with d_c being the critical thickness (~ 2 ML or 4 Å) of the spin reorientation. Since the spin reorientation occurs in the high-moment ferromagnetic region, we obtain the shape anisotropy to be of the order of 0.2 meV/atom based on the magnetization of bulk Fe. A rough estimate yields an out-of-plane anisotropy of a monolayer Fe/Cu(111) film of about -0.4 meV/atom. This value is in surprisingly good agreement with Bruno's calculation in both amplitude and sign of the anisotropy.

Finally we note that around the critical thickness where the spin reorientation of the PLD films takes place, we did not observe a drop of the Curie temperature as predicted by Bander and Mills.[25] On the contrary, the Curie temperature reached its maximum at 2 ML, i.e., the critical thickness of the spin reorientation. Above 2 ML, T_c starts to decrease gradually reaching the minimum at 6 ML above which the films transform into the bcc phase. It is surprising that the decrease of the Curie temperature takes place before the magnetic phase transformation at 3 ML, where a low-moment phase starts to form. While the change of the magnetic moment of the PLD films seems to be of structural origin, the complex behavior of the T_c needs to be further investigated.

V. SUMMARY

Using pulsed-laser deposition we are able to achieve a layer-by-layer growth of Fe on Cu(111). This growth improvement is due to the characteristic features of the PLD, in particular the extremely high instantaneous deposition rate. This technique also results in an improvement of the quality of the film structure leading to a delay of the fcc to bcc phase transformation whose critical thickness (6 ML) is twice as large as that of thermally deposited films (about 3 ML).

The magnetic behavior of the PLD films is different from that of the TD films. In the low thickness limit (<3 ML), the PLD films have long-range order and large magnetic moment while the TD films have short-range order and small magnetic moment. The easy magnetization axis of the TD films switches from perpendicular to in-plane at about 3 ML, which is clearly associated with the fcc→bcc phase transformation. In contrast, the spin reorientation of the PLD films takes place around 2 ML which is well below the critical thickness of the fcc to bcc structural phase transformation. The most striking observation with the PLD films is the magnetic phase transformation from a high-spin phase to a low-spin phase at about 3 ML, which appears to be strongly correlated with the slight decrease of the in-plane lattice constant at 3 ML.

ACKNOWLEDGMENT

The authors are grateful to G. Kroder for his technical support.

*Corresponding author. Present address: Solid State Division, Oak Ridge National Lab, Oak Ridge, TN 37831-6057.

[1] O. N. Mryasov, V. A. Gubanov, and A. I. Liechtenstein, Phys. Rev. B **45**, 12 330 (1992); M. Uhl, L. M. Sandratski, and J. Kübler, *ibid.* **50**, 291 (1994); M. Körling and J. Ergon, *ibid.* **54**, 8293 (1996).

[2] J. B. Newkirk, Trans. Am. Inst. Min., Metall. Pet. Eng. **209**, 1214 (1957).

[3] S. C. Abrahams, L. Cuttman, and J. S. Kasper, Phys. Rev. **127**, 2052 (1962); G. J. Johanson, M. B. McGirr, and D. A. Wheeler, Phys. Rev. B **1**, 3208 (1970).

[4] V. L. Moruzzi, P. M. Marcus, and J. Kubler, Phys. Rev. B **39**, 6957 (1989).

[5] R. D. Ellerbrock, A. Fuest, A. Schatz, W. Keune, and R. A. Brand, Phys. Rev. Lett. **74**, 3053 (1995).

[6] S. Müller, P. Bayer, C. Reischl, K. Heinz, B. Feldmann, H. Zillgen, and M. Wuttig, Phys. Rev. Lett. **74**, 765 (1995).

[7] J. Thomassen, F. May, B. Feldmann, M. Wuttig, and H. Ibach, Phys. Rev. Lett. **69**, 3831 (1992); Dongqi Li, M. Freitag, J. Pearson, Z. Q. Qiu, and S. D. Bader, *ibid.* **72**, 3112 (1994).

[8] D. Tian, F. Jona, and P. M. Marcus, Phys. Rev. B **45**, 11 216 (1992).

[9] W. Kümmerle and U. Gradmann, Phys. Status Solidi A **45**, 171 (1978).

[10] J. Shen, M. Klaua, P. Ohresser, H. Jenniches, J. Barthel, Ch. V. Mohan, and J. Kirschner, Phys. Rev. B **56**, 11 134 (1997).

[11] J. Shen, H. Jenniches, Ch. V. Mohan, J. Barthel, M. Klaua, P. Ohresser, and J. Kirschner, Europhys. Lett. **43**, 349 (1998).

[12] M. T. Kief and W. F. Egelhoff, Jr., Phys. Rev. B **47**, 10 785 (1993); M. T. Kief and W. F. Egelhoff, Jr., J. Vac. Sci. Technol. A **11**, 1661 (1993).

[13] A. Brodde, K. Dreps, J. Binder, Ch. Lunau, and H. Neddermeyer, Phys. Rev. B **47**, 6609 (1993); M. Klaua, H. Höche, H. Jenniches, J. Barthel, and J. Kirschner, Surf. Sci. **381**, 106 (1997).

[14] H. Jenniches, M. Klaua, H. Höche, and J. Kirschner, Appl. Phys. Lett. **69**, 3339 (1996).

[15] J. Shen, P. Ohresser, Ch. V. Mohan, M. Klaua, J. Barthel, and J. Kirschner, Phys. Rev. Lett. **80**, 1980 (1998).

[16] J. Villain, A. Pimpinelli, and D. E. Wolf, Comments Condens. Matter Phys. **16**, 1 (1992); J. Villain, A. Pimpinelli, L. Tang, and D. E. Wolf, J. Phys. I **2**, 2107 (1992).

[17] See, e.g., *Pulsed Laser Deposition of Thin Films*, edited by D. B. Chrisey and G. K. Huebler (Wiley, New York 1994).

[18] G. Rosenfeld, R. Servaty, C. Teichert, B. Poelsema, and G. Comsa, Phys. Rev. Lett. **71**, 895 (1993).
[19] J. Shen, C. Schmidthals, J. Woltersdorf, and J. Kirschner, Surf. Sci. **407**, 90 (1998).
[20] C. Rau, C. Schneider, G. Xing, and K. Jamison, Phys. Rev. Lett. **57**, 3221 (1986).
[21] P. Bruno, J. Phys. F **18**, 1291 (1988); P. Bruno, J. Appl. Phys. **64**, 3153 (1988).
[22] R. Lorenz and J. Hafner, Phys. Rev. B **54**, 15 937 (1996).
[23] S. Pick and X. Dreyssée, Phys. Rev. B **48**, 13 588 (1993).
[24] P. Bruno, Phys. Rev. B **39**, 865 (1989).
[25] M. Bander and D. L. Mills, Phys. Rev. B **38**, 12 015 (1988).